Dobslaw, H., Bergmann, I., Dill, R., Forootan, E., Klemann, V., Kusche, J., Sasgen, I. (2015): The updated ESA Earth System Model for future gravity mission simulation studies. - *Journal of Geodesy*, *89*, 5, pp. 505—513.

DOI: http://doi.org/10.1007/s00190-014-0787-8

Journal of Geodesy manuscript No.
(will be inserted by the editor)

The Updated ESA Earth System Model for Future Gravity Mission Simulation Studies

Henryk Dobslaw · Inga Bergmann-Wolf · Robert Dill · Ehsan Forootan · Volker Klemann · Jürgen Kusche · Ingo Sasgen

Received: date / Accepted: date

Abstract A new synthetic model of the time-variable global gravity field is now available based on realistic mass variability in atmosphere, oceans, terrestrial water storage, continental ice-sheets, and the solid Earth. The updated ESA Earth System Model is provided in Stokes coefficients up to degree and order 180 with a temporal resolution of 6 hours covering the time period 1995 - 2006, and can be readily applied as a source model in future gravity mission simulation studies. The model contains plausible variability and trends in both low-degree coefficients and the global mean eustatic sea-level. It depicts reasonable mass variability all over the globe at a wide range of frequencies including multi-year trends, year-to-year variability, and seasonal variability even at very fine spatial scales, which is

H. Dobslaw
Deutsches GeoForschungsZentrum GFZ, Department 1: Geodesy and Remote Sensing, Telegrafenberg, 14473 Potsdam, Germany. Tel.: +49-331-288-1974, E-mail: dobslaw@gfz-potsdam.de

I. Bergmann-Wolf
Deutsches GeoForschungsZentrum GFZ, Department 1: Geodesy and Remote Sensing, Telegrafenberg, 14473 Potsdam, Germany. Tel.: +49-331-288-1770, E-mail: ingab@gfz-potsdam.de

R. Dill
Deutsches GeoForschungsZentrum GFZ, Department 1: Geodesy and Remote Sensing, Telegrafenberg, 14473 Potsdam, Germany. Tel.: +49-331-288-1750, E-mail: dill@gfz-potsdam.de

E. Forootan
Bonn University, Institute of Geodesy and Geoinformation, Nussallee 17, 53115 Bonn, Germany. Tel.: +49-228-73-6423, E-mail: forootan@geod.uni-bonn.de

V. Klemann
Deutsches GeoForschungsZentrum GFZ, Department 1: Geodesy and Remote Sensing, Telegrafenberg, 14473 Potsdam, Germany. Tel.: +49-331-288-1104, E-mail: volkerk@gfz-potsdam.de

J. Kusche
Bonn University, Institute of Geodesy and Geoinformation, Nussallee 17, 53115 Bonn, Germany. Tel.: +49-228-73-2629, E-mail: jkusche@geod.uni-bonn.de

I. Sasgen
Deutsches GeoForschungsZentrum GFZ, Department 1: Geodesy and Remote Sensing, Telegrafenberg, 14473 Potsdam, Germany. Tel.: +49-331-288-1145, E-mail: sasgen@gfz-potsdam.de

important for a realistic representation of spatial aliasing and leakage. In particular on these small spatial scales between 50 and 250 km, the model contains a range of signals that have not been reliably observed yet by satellite gravimetry. In addition, the updated Earth System Model provides substantial high-frequency variability at periods down to a few hours only, thereby allowing to critically test strategies for the minimization of temporal aliasing.

Keywords Time-Variable Gravity Field · Future Satellite Gravity Missions · GRACE-FO

1 Introduction

The accuracy of satellite observations of the Earth's gravity field has progressed rather rapidly during the last decade with the successful operation of the three dedicated missions CHAMP (*Reigber et al.*, 2002), GRACE (*Tapley et al.*, 2004b), and GOCE (*Rummel et al.*, 2011). The time-mean or static component of the Earth's gravity field has been surveyed globally with an approximate accuracy of 1 cm at spatial wavelengths of about 100 km, which is roughly two orders of magnitude more accurate than one of the most recent global gravity field models based on Satellite Laser Ranging data only (*Biancale et al.*, 2000).

In addition, time-variable gravity field solutions are available from GRACE for about twelve years now, which reflect mass redistributions in the Earth system on large spatial scales down to a few 100 km. These unique observations allow for the first time the quantification of terrestrially stored water mass variability (*Tapley et al.*, 2004a), the monitoring of continental ice-mass changes including their contribution to changes in sea-level (*Velicogna and Wahr*, 2006), or the detection of co-seismic displacements associated with major earthquakes (*Han et al.*, 2006). In 2014, the GRACE mission is still in operation and delivers monthly mean gravity field models with an typical latency of about 60 days, even though battery degradation requires the switch-off of the science instruments every 161 days for about 3 to 4 weeks.

In order to continue the time-series of large-scale mass variability obtained with GRACE, a follow-on mission is currently being realized under a U.S.-German partnership (*Flechtner et al.*, 2014). GRACE-FO will be based largely on well-tested components already implemented in the GRACE mission. In addition to a GRACE-type microwave inter-satellite link with a typical range-rate precision of 0.2 μm/s, a laser interferometer is included into the GRACE-FO payload as a science demonstrator instrument, which is expected to provide range-rates between the two satellites down to a precision of about 1 nm/s. Thereby, GRACE-FO is expected to deliver additional information on finer spatial scales of the time-variable gravity field. The follow-on mission is scheduled for launch in August 2017 and will have a nominal life-time of seven years (*Flechtner et al.*, 2014).

To further extend our knowledge about the Earth's external gravity field with the help of satellite observations, there are three fundamentally different options for increasing the sensitivity of a future mission beyond the GRACE-FO level (*Rummel*, 2003). These are (i) the choice of a very low experiment altitude, which even might require active drag compensation; (ii) a compensation of field attenuation by differential measurements, be it aboard a single satellite as realized with

GOCE, or as a constellation of multiple satellites with inter-satellite links; and (iii) an increase in measurement precision of the actual science instruments, most notably the range-rate measurement device and the accelerometers.

To trade-off those options for a maximum scientific return at reasonable overall mission expenses, extensive simulation studies are typically performed by different research groups (*Visser*, 2010; *Wiese et al.*, 2011; *Loomis et al.*, 2011; *Elsaka et al.*, 2014). Such studies usually start from simulated orbits based on a source model of global mass variability, proceed to the retrieval of time-series of global gravity field models including some strategy for mitigating the effects of mass variability at time-scales below the analysis interval, and finally apply appropriate post-processing filters or inversion techniques to obtain surface mass densities which are to be compared again to the source model applied in the initial orbit simulation step. For such simulation studies, it is critically important to have included realistic mass variability at all relevant spatial and temporal scales into the source model, since otherwise the performance of a candidate mission concept cannot be tested thoroughly and conclusions drawn from such simulations are certainly too optimistic.

In this short note, we present a new synthetic model of the time-variable gravity field with both high spatial and temporal resolution that extends over a period of 12 years. The underlying geophysical models that provide the mass variability in atmosphere, oceans, the terrestrial water storage, the continental cryosphere, and the solid Earth are described in Section 2. Time-variations of selected low-degree coefficients (Section 3) and the eustatic global mean sea-level (Section 4) are discussed, before the signal content of this new source model is assessed globally for different parts of the temporal spectrum, i.e., the linear trends (Section 5), the year-to-year variability (Section 6), the seasonal variability (Section 7), and the high-frequency part (Section 8). Details on data access and available documentation are provided in Section 9, before a brief summary is given in the final Section 10.

2 Components of the Updated ESM

The new synthetic model of the time-variable gravity field presented here is delivered in five separate components that individually describe mass variability in atmosphere (A component), oceans (O component), continental ice-sheets (I component), terrestrially stored water (H component), and the solid Earth (S component). Developed under a contract with the European Space Agency (ESA), the model is intended to update an earlier model published by *Gruber et al.* (2011), which we refer to as the original Earth System Model (ESM) in the remainder of this paper. Like its predecessor, the updated ESM covers a time-period of 12 years (1995 - 2006) with a temporal resolution of 6 hours and a spatial resolution of maximum spherical harmonic degree and order 180.

For the atmospheric part of the updated ESM, we use the latest re-analysis from ECMWF, ERA-Interim (*Dee et al.*, 2011). It is currently available from 1979 - 2014 and represents a synthesis of multiple types of observations describing the evolution of the atmosphere over the last decades. Although the physical model, the numerical scheme, and the data assimilation framework of ERA-Interim remain unmodified during the whole re-analysis period, systematic biases related to changes in the observational network or caused by volcano-induced atmospheric disturbances that lead to modifications in the calibration parameters of satellite radiances cannot be excluded. Compared to other available re-analysis data sets, however, ERA-Interim performs favourably well, in particular with respect to the representation of the atmospheric branch of the terrestrial water cycle (*Lorenz and Kunstmann*, 2012; *Springer et al.*, 2014).

The cryospheric component of the updated ESM is based on results from two configurations of the regional climate model RACMO (*Ettema et al.*, 2009) that provide high-resolution estimates of individual components of the surface mass balance – precipitation, evaporation and sublimation, as well as run-off, melting and re-freezing – of glaciated regions in both Greenland and Antarctia. The model is forced at its lateral boundaries and at the sea-surface with ERA-Interim data, and runs at a spatial resolution of 11 km. Surface mass balance variations are calculated as cumulative anomalies w.r.t. the period 1995 - 2006. The ice discharges used for the update, however, remain identical to those applied in the original ESM. In that previous work, secular trends in ice dynamics were imposed for areas of different outlet glaciers in Greenland and Antarctica with observed surface velocities higher than 50 m a^{-1}. Starting from 1998 onwards, increased ice discharge and ablation has been imposed, which results in a roughly constant loss of 110 Gt a^{-1} to the oceans (*Gruber et al.*, 2011).

Forced with atmospheric freshwater and energy fluxes from ERA-Interim, the Land Surface Discharge Model (LSDM; *Dill*, 2008) simulates vertical and horizontal water transport and storage on land surfaces. Physics and parametrisation of LSDM are based on *Hagemann and Dümenil* (1998, 2003), and include the representation of soil moisture, snow storage, and water stored in wetlands, rivers, and lakes. The model is discretized on a 0.5° equiangular grid and provides mass estimates at daily time intervals. LSDM is in particular well suited to study spatial aliasing effects in time-variable gravity field retrievals, since it includes mass anomalies advected in the river channels which are often distinctly different compared to the mass anomalies related to the surrounding soil moisture or snow cover. In addition, LSDM contains a parametrisation for the antropogenic water management at Lake Nasser (Egypt), leading to highly concentrated water mass variations in the hydrologic part of the updated ESM at this location in the Nile catchment.

The oceanic part of the updated ESM is essentially the sum of three different contributions. First, the Ocean Model for Circulation and Tides (OMCT; *Thomas et al.*, 2001) in a setting that is also used for the latest version of the official GRACE De-Aliasing Product (AOD1B; *Flechtner and Dobslaw*, 2013) provides high-frequency variability at the large spatial scales. Compared to both satellite altimetry and deep-sea pressure gauges, this model performs favourably well in explaining mass variability at periods below 30 days (*Dobslaw et al.*, 2013). Secondly, meso-scale variability not simulated by OMCT is taken for d/o > 60 from the high-resolution STORM experiment performed with the MPIOM ocean model (*Storch et al.*, 2012), which shares with OMCT its heritage from the Hamburg Ocean Primitive Equation model HOPE (*Wolff et al.*, 1997). Thirdly, a uniform layer of sea-level is added in order to balance the summarized mass anomalies in atmosphere, cryosphere, and continental water storage in a way that the total mass in the Earth system remains constant at all times.

Finally, deformations of the solid Earth in response to ongoing glacial isostatic adjustment (GIA) in Fennoscandia, Laurentide, and the West-Antarctic are taken from the original ESM (*Gruber et al.*, 2011). Since this model did not include degree-1 contributions, these are now included following *Klemann and Martinec* (2011). As an example for an incidental major seismic event, a model representation of co- and post-seismic deformations resulting from the magnitude 9.1 Sumatra-Andaman earthquake is included into the solid Earth part of the updated model in a very similar way as it has been done for the original ESM.

3 Low-Degree Harmonics

To demonstrate the long-term stability of the updated ESM, we add the individual components A, O, H, I, and S to arrive at a summarized component AOHIS, and display time-series of low-degree harmonics of this component for both the original and the updated ESM (Fig. 1). For the total mass of the Earth, we note a trend of about 3 mm a^{-1} in terms of geoid height in the original ESM, which is obviously unrealistic. Analysis of the individual components indicate that this mass increase is particularly driven by the simulated continental water storage variability of *Gruber et al.* (2011). For the updated ESM, variations in total mass are practically zero: we only find a remaining trend of $8 \cdot 10^{-5}$ mm a^{-1}, and a standard deviation of $4 \cdot 10^{-4}$ mm for C_{00}.

For the z component of the geocenter position as reflected in C_{10}, we note a rather strong trend of 0.75 mm a^{-1} in the original ESM, which is partly related to a sudden jump by about 10 mm on January 1st, 2006. No such features are present in the updated ESM with a trend in C_{10} of -0.14 mm a^{-1}, and a standard deviation of 1.7 mm. Trends in this coefficient are primarily caused by the solid Earth, but continental ice-mass changes also contribute by a substantial amount.

For the coefficient C_{20} describing the dynamic flattening of the Earth we find once more a sudden shift on January 1st, 2006 in combination with a substantial drift over the whole model period in the original ESM. For the updated model, the linear trend in C_{20} is practically zero (0.04 mm a^{-1}), since contributions from ice and solid Earth components cancel each other almost perfectly. More details on the temporal behaviour of low-degree coefficients from the individual components A, O, H, I, and S, and their comparison against *Gruber et al.* (2011) are given in *Bergmann-Wolf et al.* (2014a).

4 Eustatic Sea-Level Variability

Global mean eustatic sea-level is a key quantity currently observed with GRACE, and it should be represented realistically also in any Earth System Model for future gravity mission simulation studies. For the seasonal cycle, we note large year-to-year variability in the original ESM (Fig. 2) which is not supported by the currently available GRACE record. The seasonal cycle of the updated ESM instead agrees in its phase (peak at 278 days) quite well with GRACE (peak at 288 days; *Bergmann-Wolf et al.*, 2014b), but the annual amplitude is with 6.3 mm substantially smaller in the new model when compared to the observations.

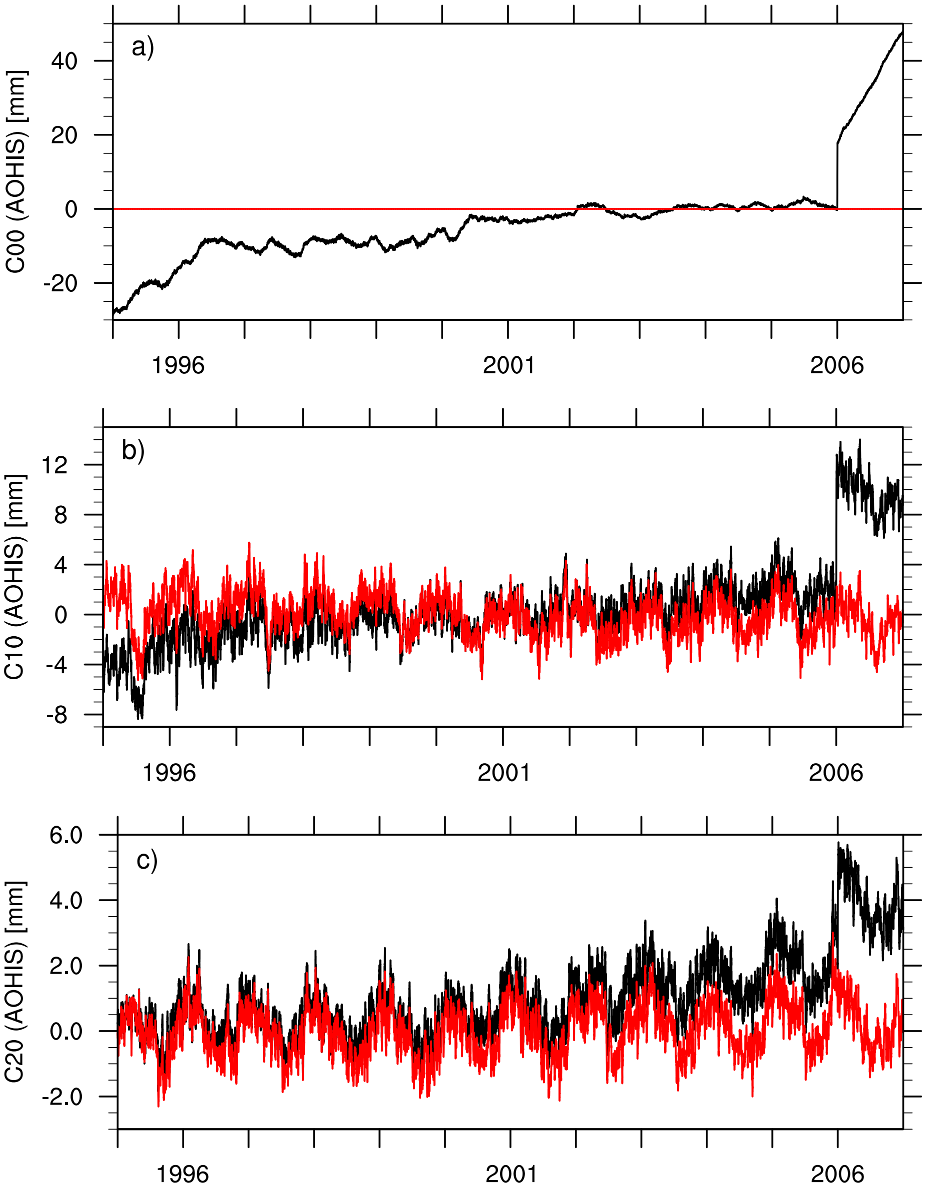

Fig. 1 Time-series of low-degree harmonics C_{00} (a), C_{10} (b), and C_{20} (c) for the summarized components AOHIS of the original (black) and the updated ESM (red) in terms of geoid heights [mm] over the whole 12 year model period.

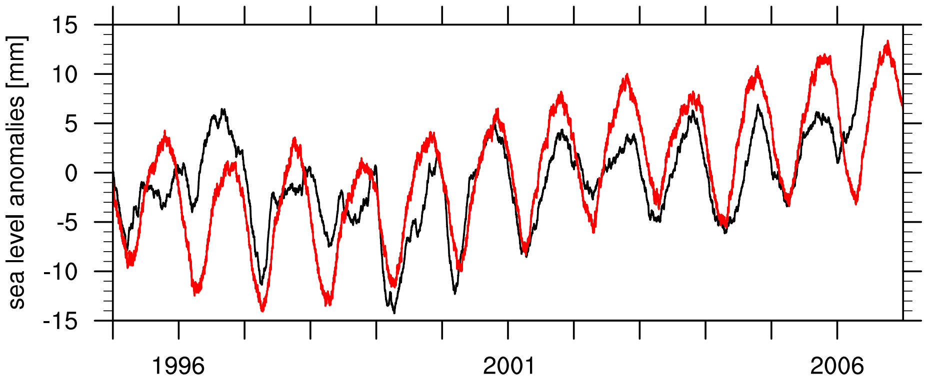

Fig. 2 Time-series of global mean eustatic sea-level anomalies [cm] derived from the original (black) and the updated ESM (red) over the whole 12 year model period.

For the low-frequency part of the spectrum, however, both ESM data-sets largely agree with each other by showing a period of almost constant eustatic sea-level between 1995 and 1998, followed by a rapid acceleration towards a global mean eustatic sea-level rise of about 1.3 mm a^{-1}. For the whole 12 year time-period, this averages to a linear trend of 0.98 mm a^{-1} in the updated ESM. Even though it might be debatable whether or not such a rapid acceleration in sea-level has taken place in reality during that time, it is important to have such a signal included into the ESM in order to test to what accuracy a future mission candidate might be able to detect such accelerations, which potentially might have a very high impact on coastal societies.

5 Linear Trends

For our further analysis, we utilize the five individual components A, O, H, I, and S of the updated ESM at 6 hourly resolution, synthesize the coefficients up to d/o = 180 onto a 0.5° latitude-longitude grid, calculate daily averages, and summarize A and O as well as H, I, and S into two summarized components AO and HIS, respectively. We empirically de-trend the grids, and filter the residuals with a 3rd order Butterworth filter at two different cut-off periods of 30 and 365 days. Thereby, we obtain three band-limited time-series that reflect year-to-year variability (i.e., at periods between 1 and 12 years), seasonal variability (i.e., at periods between 1 and 12 months), and high-frequency variability (i.e., at periods between 1 and 30 days), whose characteristics will be discussed below.

Linear trends estimated from the AO component of the updated ESM are largely dominated by a globally homogeneous signal of about 0.1 hPa a^{-1}, which is roughly equivalent to a 1 mm a^{-1} rise in global mean eustatic sea-level (Fig. 3a). Overlaid is an additional increase in ocean bottom pressure in the sub-tropical North Pacific, where low-frequency changes in the surface winds cause associated bottom pressure changes at rates of about 0.3 hPa a^{-1}. Trends in surface pressure over the continents are typically smaller than 0.2 hPa a^{-1} and rather large-scale,

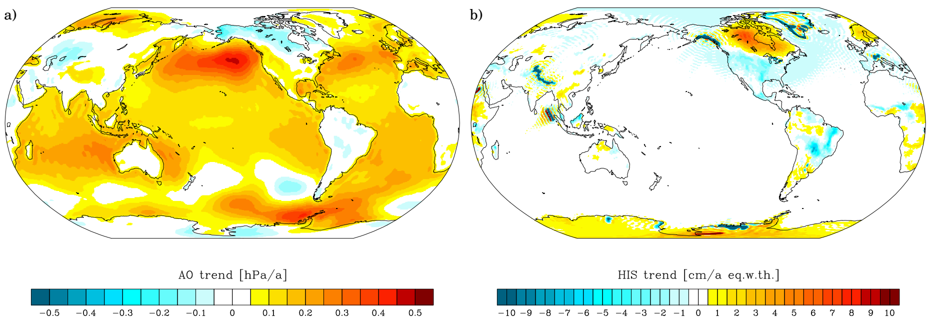

Fig. 3 Linear trends of components AO (a) and HIS (b) of the updated ESM calculated over the period 1995 - 2006.

reflecting small changes in the climatological long-term mean of the atmospheric circulation.

Instead, linear trends of the HIS component are more than one magnitude larger (Fig. 3b). Mass redistributions related to GIA at the center of the former Laurentide ice-dome in North America reach rates that correspond to a yearly surface mass density increase of up to 7 cm equivalent water thickness (eq. w. th.), which is approximately equivalent to a pressure change of 7 hPa. In addition, shrinking of both continental ice-sheets and various mountain glaciers causes mass loss rates of up to 10 cm a^{-1} eq. w. th., but those signals vary rather strongly over small distances: outlet glaciers in Antarctica and Greenland are therefore easily discernable.

In contrast to the characteristics of the ice mass changes, we find trends in the terrestrially stored water to be rather small (i.e., 3 cm a^{-1} eq. w. th.) but consistent over larger areas, since effects like groundwater withdrawal for human consumption and irrigation are not included in this model. The updated ESM thereby contains both strong trends with rather small spatial extent as well as very weak trends at larger spatial scales. Both features are challenging to recover accurately for future mission candidates.

We also note a strong trend signal at the position of the Sumatra-Andaman earthquake in the HIS component. Co-seismic deformation is modeled in the updated ESM as a step function, followed by a linear post-seismic deformation over exactly 1 year. Fitting a straight line to the 12 year data period covering the step will yield an estimate for the trend different from zero, even though the exact value is largely depending on the length of the period considered. Similar arguments are in place for effects of step functions on empirically derived estimates of temporal variability from band-limited data. We will therefore not further discuss any signals related to the earthquake in the remainder of this paper.

6 Year-to-Year Variability

De-trended signals that are low-pass filtered with a 365 days cut-off period reveal variability in the AO component of the updated ESM of a few hPa (Fig. 4a). Strongest standard deviations of around 4 hPa appear over Greenland and

Antarctica, whereas those of tropical regions are typically only 1 hPa. Over the oceans, we note an isolated signal of 8 hPa in the Baltic, and rather large-scale pattern of enhanced variability in several sub-basins of the extra-tropical Pacific of around 3 hPa.

For the HIS component (Fig. 4b), we find substantially larger variabilities with maximum values of more than 30 cm along the Amazon river, and with about 25 cm eq. w. th. over Lake Nasser in Egypt. Isolated peaks with similar magnitude are also apparent at the locations of several outlet glaciers in both Antarctica and Greenland, as well as in low-latitude regions under monsoon influence, as, for example, in South-East Asia.

Exemplarily, we show the annual mean of the de-trended and low-pass filtered variability over the year 2006 in order to provide evidence on the spatial correlation characteristics of the signals. For the AO component (Fig. 4c), we note atmospheric pressure anomalies that are rather coherent over large spatial scales, in particular for areas at similar altitudes. For the oceans, coherent wind-driven signals with large decorrelation lengths are additionally overlaid by meso-scale variability. With maximum absolute values of about 3 hPa, however, all those signals are relatively modest.

For the HIS component instead, maximum absolute values of 25 cm of water are in particular located in humid catchments of the tropics (Fig. 4d). Signals are more regionally variable and frequently uncorrelated to those from neigboring places which have a different hydroclimate. It will be interesting to study at which accuracy and resolution a future mission candidate is able to separate the year-to-year water storage variability of the Parana catchment from those of the southern tributaries of the Amazon, and, for example, Rio Tocantins. Since such signals are particularly important for the quantification of local water availability in response to both natural climate variability and antropogenic effects, it is rather important to reliably discriminate such closely co-located signals with a future gravity mission.

7 Seasonal Variability

Seasonal variability as obtained by bandpass-filtering with 365 and 30 days cut-off periods reaches up to 9 hPa for atmospheric pressure in high latitudes of the Northern Hemisphere (Fig. 5a). These signals are roughly equal in amplitude to the mass variability seen in the HIS component at similar regions (Fig. 5b). Oceanic signals are generally smaller, but still reach about 6 hPa in the Bellingshausen Basin in the Southeast Pacific.

Once more, we exemplarily show the monthly mean mass variability for March 2006 of the band-pass filtered signals for both the AO (Fig. 5c) and the HIS component (Fig. 5d). Monthly mean atmospheric mass anomalies are highly coherent over spatial scales of several thousands of km, whereas terrestrial water storage anomalies are more variable, in particular in relation to an apparent contrast between surface water mass stored in rivers, lakes, or reservoirs, and water stored in the soil or the snow pack. Those contrasts are a potential source of spatial aliasing in future mission gravity field retrievals, which should be attempted to be kept small to allow for reliable estimates also on regional scales.

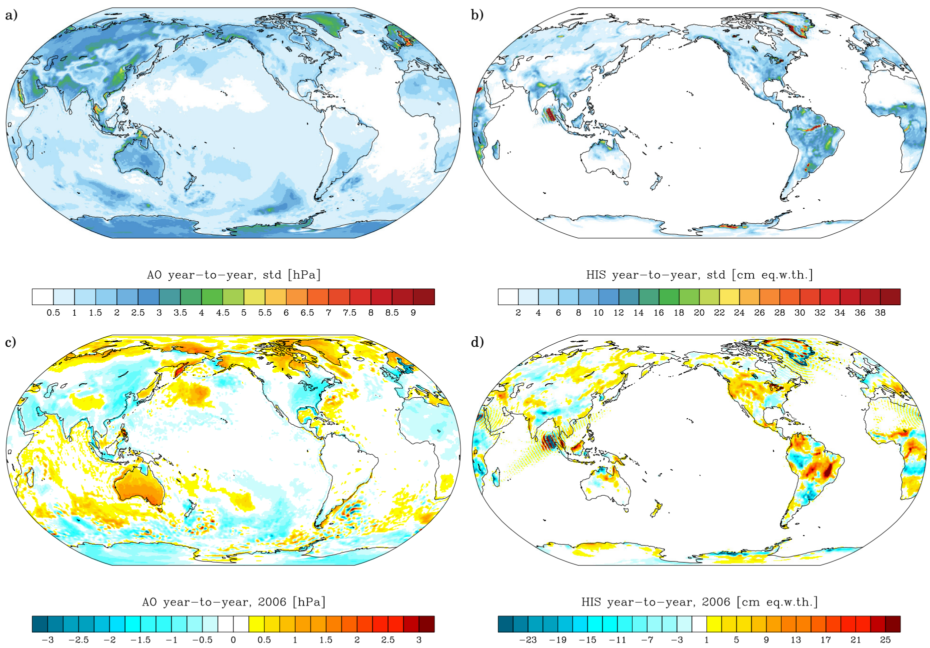

Fig. 4 Standard deviation of year-to-year-filtered variability of the components AO (a) and HIS (b) as well as year-to-year-filtered anomalies of the components AO (c) and HIS (d) of the year 2006 of the updated ESM.

8 High-Frequency Variability

High-frequency variability contained in the updated ESM is finally separated by applying a high-pass filter with 30 days cut-off period. Standard deviations of atmospheric variability reach up to 10 hPa at higher latitudes (Fig. 6a), whereas pressure variability in the tropics remains below 2 hPa as long as sub-diurnal variability and atmospheric tides are excluded. Ocean bottom pressure variability is dominated by peak values in resonant basins of the Southern Ocean, in marginal seas, and in shallow shelf areas. Most of these signals are, however, rather large-scale as illustrated by an arbitrarily selected example of AO high-frequency mass anomalies (Fig. 6c), thereby opening opportunities to capture them with sufficient accuracy by increasing the number of observations in a future gravity mission constellation.

Compared to atmosphere and ocean variability, we note rather small high-frequency signals of only 2 cm eq. w. th. in the HIS component (Fig. 6b). Those are primarily related to the onset of major precipitation events (Fig. 6d), and would provide a very useful benchmark signal for a future gravity mission when aiming at validation and calibration of evaporation products through solving the terrestrial water balance equation at shorter time-scales. In view of the much larger atmospheric signals, it remains, however, questionable whether a reliable separation of high-frequency water storage variability from residual atmospheric

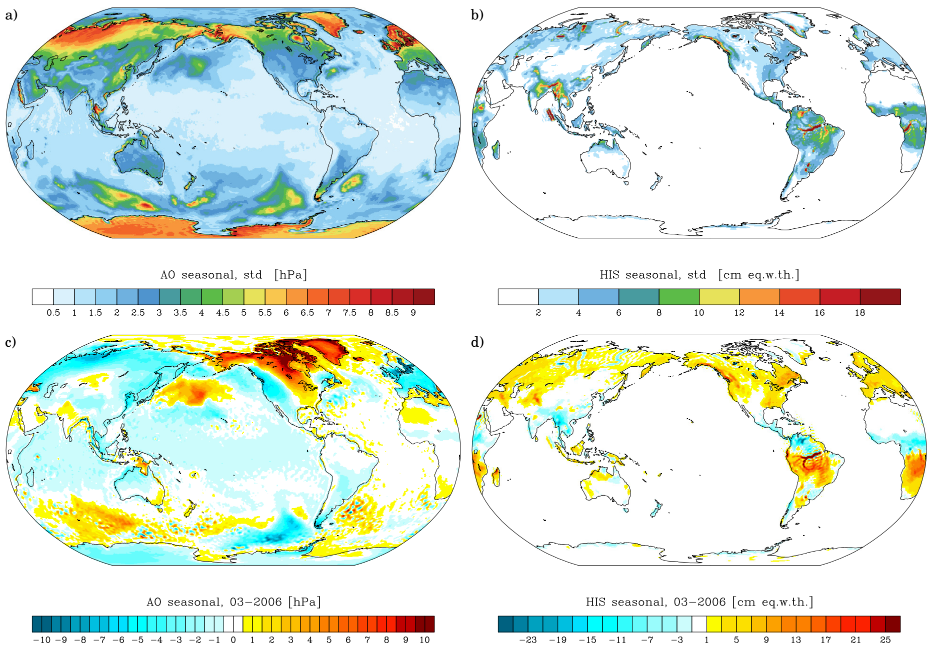

Fig. 5 Standard deviation of seasonal-filtered variability of the components AO (a) and HIS (b) as well as seasonal-filtered anomalies of the components AO (c) and HIS (d) of March 2006 of the updated ESM.

pressure signals and all kinds of errors present in the finally retrieved time-variable gravity fields will be eventually possible.

In addition to the high-frequency variabilty discussed above, the 6 hourly-sampled ESM data-set also contains variability at sub-diurnal frequencies including atmospheric tides and their oceanic response. There are, however, no signals at periods shorter than one day in the other components H, I, and S. Readers interested in those very rapid signals in atmosphere and oceans are referred to the chapters 10 and 11 of *Dobslaw et al.* (2014).

9 Data Access and Documentation

The complete data-set of the updated ESM is publicly available at DOI: 10.5880/GFZ.1.3.2014.001. A detailed documentation of the updated ESM that also includes validation against numerous observations is provided by *Dobslaw et al.* (2014). An in-depth comparison with the original ESM is given in *Bergmann-Wolf et al.* (2014a). The Stokes coefficients of the updated ESM are provided as individual components A, O, H, I, and S, and as summarized component AOHIS. In addition, an atmospheric component without applying the modified IB correction (AnoIB) is provided over the whole 12 year period. For the year 2006, all components are additionally delivered at higher spatial (d/o = 360) and temporal (3 h) resolution. For the same year, we are also offering an alternative atmospheric

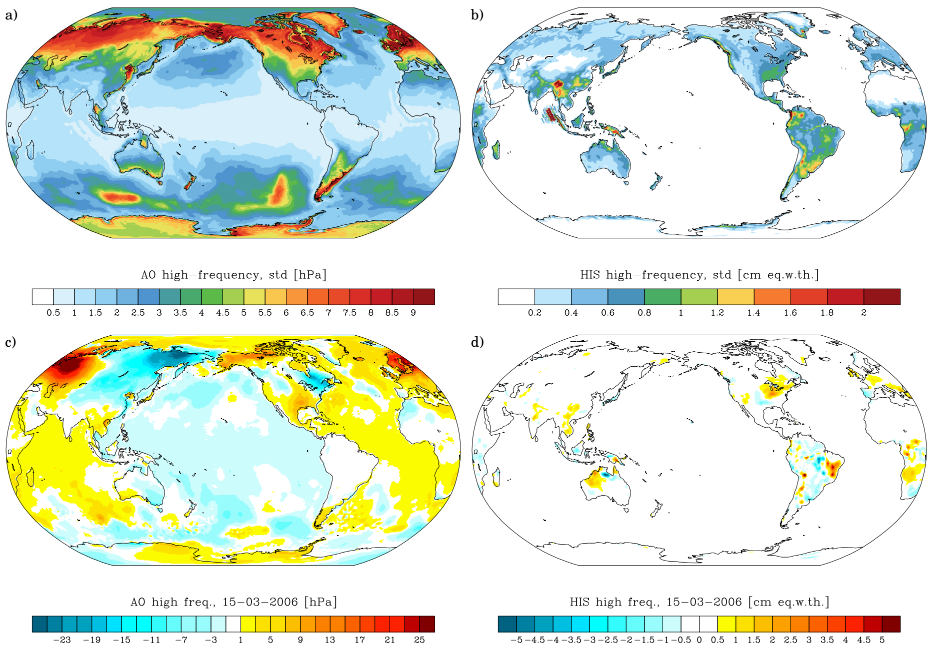

Fig. 6 Standard deviation of high-frequency-filtered variability of the components AO (a) and HIS (b) as well as high-frequency-filtered anomalies of the components AO (c) and HIS (d) of March 15th, 2006 of the updated ESM.

component (Ac) with the high-resolution atmospheric model COSMO-EU blended into ERA-Interim over Europe. Further details on those accompanying sets of coefficients are given in *Dobslaw et al.* (2014).

10 Summary

A new synthetic model of the time-variable global gravity field is now available for satellite gravity mission simulation studies. The updated ESA Earth System Model spans 12 years (1995 - 2006) with a temporal resolution of 6 hours and a spatial resolution of spherical harmonic degree and order 180. It describes mass variability in atmosphere, oceans, the terrestrially stored water including the continental ice-sheets, as well as deformations of the solid Earth on a wide range of temporal frequencies, which is generally consistent with the knowledge acquired during the GRACE mission period.

In contrast to its predecessor, the original ESM of *Gruber et al.* (2011), the updated ESM is approximately stationary over all 12 years for a number of different frequency bands, and therefore allows to principally compare simulation results for different years with each other. It also allows to compare different future mission candidates with respect to their ability to detect linear trends related to GIA, accelerations in ice mass loss for Greenland and Antarctica, year-to-year variability in the terrestrially stored water in response to natural climate variability, or seasonal variations due to the alternation of dry and wet periods in areas affected by Monsoon dynamics. These assessments are possible from the evaluation of results from a single multi-year simulation experiment only, so that potential trade-offs between different competing scientific requirements can be assessed in a straight-forward way.

At the same time, the updated ESM is challenging for any future mission candidate in terms of realism by providing substantially higher spatial resolution of mass variability for all those processes than currently available from GRACE. Water storage anomalies dominated by surface water in the updated ESM, for example, are typically distinctly different from neighboring soil moisture or snow storage anomalies. Meso-scale variability included into the ocean component provides steep spatial gradients in ocean bottom pressure, and local mass trends of Greenland's major outlet glaciers have different signal characteristics than those of ice masses nearby. Based on the configuration of a future mission candidate and the gravity field retrieval method chosen, those small-scale features will cause different levels of spatial aliasing and leakage, which is currently perceived as one of the major obstacles for a wider dissemination of the present-day GRACE results.

In addition, the updated ESM also contains substantial variability on very short periods from hours to days in atmosphere, oceans and – to a much smaller extent – also in the terrestrially stored water. These signals are important for testing strategies for the reduction of temporal aliasing, and will play a key role in assessing the added value of mission configurations with two or even more pairs of satellites in presumably differently inclined orbits.

Although effects of temporal aliasing can be reduced by means of additional observations from multiple pairs of satellites, it is currently still necessary to introduce a priori knowledge about high-frequency variability in atmosphere and oceans by means of time-variable background models as the GRACE AOD1B product (*Flechtner and Dobslaw*, 2013). Those models are inevitably incomplete and contain errors correlated in time and space that contribute substantially to the overall error budget of present-day gravity missions. Future work will therefore concentrate on the preparation of a realistically perturbed de-aliasing model, which is consistent with the updated ESM presented here.

Acknowledgements This study was performed under contract No. 4000109421 with the European Space Agency (ESA). We thank M. R. van den Broeke for provinding output of RACMO2. We also thank Deutscher Wetterdienst, Offenbach, Germany, and the European Centre for Medium-Range Weather Forecasts, Reading, U.K., for providing data from ECMWF's latest re-analysis ERA-Interim. Numerical simulations were performed at Deutsches Klimarechenzentrum, Hamburg, Germany.

References

Bergmann-Wolf, I., R. Dill, E. Forootan, V. Klemann, J. Kusche, I. Sasgen, and H. Dobslaw (2014a), Updating ESAs Earth System Model for Gravity Mission Simulation Studies: 2. Comparison with the Original Model, *Tech. rep.*, Scientific Technical Report 14/08, GFZ, Potsdam, doi:10.2312/GFZ.b103-14088.

Bergmann-Wolf, I., L. Zhang, and H. Dobslaw (2014b), Global Eustatic Sea-Level Variations for the Approximation of Geocenter Motion from Grace, *Journal of Geodetic Science*, *4*(1), 37–48, doi:10.2478/jogs-2014-0006.

Biancale, R., et al. (2000), A new global Earth's gravity field model from satellite orbit perturbations: GRIM5-S1, *Geophys. Res. Lett.*, *27*(22), 3611–3614.

Dee, D. P., et al. (2011), The ERA-Interim reanalysis: configuration and performance of the data assimilation system, *Q. J. Roy. Met. Soc.*, *137*(656), 553–597, doi:10.1002/qj.828.

Dill, R. (2008), Hydrological model LSDM for operational Earth rotation and gravity field variations Hydrological, *Tech. rep.*, Scientific Technical Report 08/09, GFZ, Potsdam, doi:11.2312/GFZ.b103-08095.

Dobslaw, H., F. Flechtner, I. Bergmann-Wolf, C. Dahle, R. Dill, S. Esselborn, I. Sasgen, and M. Thomas (2013), Simulating high-frequency atmosphere-ocean mass variability for dealiasing of satellite gravity observations: AOD1B RL05, *J. Geophys. Res.*, *118*(7), 3704–3711, doi:10.1002/jgrc.20271.

Dobslaw, H., I. Bergmann-Wolf, R. Dill, E. Forootan, V. Klemann, J. Kusche, and I. Sasgen (2014), Updating ESAs Earth System Model for Gravity Mission Simulation Studies: 1. Model Description and Validation, *Tech. rep.*, Scientific Technical Report 14/07, GFZ Potsdam, Potsdam, doi:10.2312/GFZ.b103-14079.

Elsaka, B., J.-C. Raimondo, P. Brieden, T. Reubelt, J. Kusche, F. Flechtner, S. Iran Pour, N. Sneeuw, and J. Müller (2014), Comparing seven candidate mission configurations for temporal gravity field retrieval through full-scale numerical simulation, *J. Geodesy*, *88*(1), 31–43, doi:10.1007/s00190-013-0665-9.

Ettema, J., M. R. van den Broeke, E. van Meijgaard, W. J. van de Berg, J. L. Bamber, J. E. Box, and R. C. Bales (2009), Higher surface mass balance of the Greenland ice-sheet revealed by high-resolution climate modeling, *Geophys. Res. Lett.*, *36*(12), L12,501, doi:10.1029/2009GL038110.

Flechtner, F., and H. Dobslaw (2013), GRACE AOD1B Product Description Document for Product Release 05, *Tech. rep.*, Rev. 4.0, GRACE Document 327-750, GeoForschungsZentrum Potsdam.

Flechtner, F., P. Morton, M. Watkins, and F. Webb (2014), Status of the GRACE Follow-On Mission, in *IAG Symposium Gravity, Geoid, and Height Systems*, pp. IAGS–D–12–00,141.

Gruber, T., et al. (2011), Simulation of the time-variable gravity field by means of coupled geophysical models, *Earth System Science Data*, *3*(1), 19–35, doi:10.5194/essd-3-19-2011.

Hagemann, S., and L. Dümenil (1998), A parametrization of the lateral waterflow for the global scale, *Climate Dynamics*, *31*(14), 17–31.

Hagemann, S., and L. Dümenil (2003), Improving a subgrid runoff parameterization scheme for climate models by the use of high-resolution data derived from satellite observations, *Climate Dynamics*, *21*(3-4), 349–359, doi:10.1007/s00382-003-0349-x.

Han, S., C. Shum, M. Bevis, C. Ji, and C. Kuo (2006), Crustal dilatation observed by GRACE after the 2004 Sumatra-Andaman earthquake, *Science*, *313*, 658–662.

Klemann, V., and Z. Martinec (2011), Contribution of glacial-isostatic adjustment to the geocenter motion, *Tectonophysics*, *511*(3-4), 99–108, doi:10.1016/j.tecto.2009.08.031.

Loomis, B. D., R. S. Nerem, and S. B. Luthcke (2011), Simulation study of a follow-on gravity mission to GRACE, *J. Geodesy*, *86*(5), 319–335, doi:10.1007/s00190-011-0521-8.

Lorenz, C., and H. Kunstmann (2012), The hydrological cycle in three state-of-the-art reanalyses: intercomparison and performance analysis, *Journal of Hydrometeorology*, *13*, 1397–1420.

Reigber, C., et al. (2002), A High-Quality Global Gravity Field Model from CHAMP GPS Tracking Data and Accelerometry (EIGEN1S), *Geophys. Res. Lett.*, *29*(14), 94–97.

Rummel, R. (2003), How to climb the gravity wall, *Space Science Reviews*, *108*(1-2), 1–14.

Rummel, R., W. Yi, and C. Stummer (2011), GOCE gravitational gradiometry, *J. Geodesy*, *85*(11), 777–790, doi:10.1007/s00190-011-0500-0.

Springer, A., J. Kusche, K. Hartung, C. Ohlwein, and L. Longuevergne (2014), New Estimates of Variations in Water Flux and Storage over Europe Based on Regional (Re)Analyses and Multisensor Observations, *Journal of Hydrometeorology*, pp. 1–54, doi:10.1175/JHM-D-14-0050.1.

Storch, J.-S. V., C. Eden, I. Fast, H. Haak, D. Hernández-Deckers, E. Maier-Reimer, J. Marotzke, and D. Stammer (2012), An Estimate of the Lorenz Energy Cycle for the World Ocean Based on the STORM/NCEP Simulation, *J. Phys. Oceanogr.*, *42*(12), 2185–2205, doi:10.1175/JPO-D-12-079.1.

Tapley, B. D., S. Bettadpur, J. C. Ries, P. F. Thompson, and M. Watkins (2004a), GRACE measurements of mass variability in the Earth system., *Science*, *305*(5683), 503–5, doi:10.1126/science.1099192.

Tapley, B. D., S. Bettadpur, M. Watkins, and C. Reigber (2004b), The gravity recovery and climate experiment: Mission overview and early results, *Geophys. Res. Lett.*, *31*(22), 09,607, doi:10.1029/2004GL019920.

Thomas, M., J. Sündermann, and E. Maier-Reimer (2001), Consideration of ocean tides in an OGCM and impacts on subseasonal to decadal polar motion, *Geophys. Res. Lett.*, *28*(12), 2457–2460.

Velicogna, I., and J. Wahr (2006), Acceleration of Greenland ice mass loss in spring 2004., *Nature*, *443*(7109), 329–31, doi:10.1038/nature05168.

Visser, P. N. A. M. (2010), Designing Earth Gravity Field Missions for the Future: A Case Study, in *IAG Commission 2: GRAVITY, GEOID AND EARTH OBSERVATION, Chania (Greece)*, pp. 131–138.

Wiese, D. N., R. S. Nerem, and F. G. Lemoine (2011), Design considerations for a dedicated gravity recovery satellite mission consisting of two pairs of satellites, *J. Geodesy*, *86*(2), 81–98, doi:10.1007/s00190-011-0493-8.

Wolff, J.-O., E. Maier-Reimer, and S. Legutke (1997), *The Hamburg Ocean Primitive Equation Model*, 13, 1–110 pp., DKRZ.